J Appl Electrochem (2010) 40:1483–1491
DOI 10.1007/s10800-010-0127-5

ORIGINAL PAPER

Corrosion inhibition efficiency study in a microalloyed steel for sour service at 50 °C

A. Torres-Islas · S. Serna · J. Uruchurtu · B. Campillo · J. G. González-Rodríguez

Received: 6 October 2009 / Accepted: 27 March 2010 / Published online: 16 April 2010

Abstract A H_2S corrosion inhibition efficiency study by a carboxyamidoimidazoline compound was carried out using electrochemical impedance spectroscopy (EIS) and electrochemical noise (EN) techniques. The microalloyed steel assessed was specially designed for sour gas transport and is intended to be applied as line pipe steel in Mexico. The corrosive media was a deaerated 3% NaCl solution, H_2S saturated after heated to 50 °C, with several inhibitor concentrations, ranging from 0 to 100 ppm, per test. The EIS and ENA data were analyzed and use as monitoring indicators for the development of a protective film by the inhibitor within 24 h testing. The results indicate that maximum inhibitor efficiency was achieved with only 5 ppm inhibitor concentration, but this efficiency value decreases with increasing of the inhibitor concentration. In addition the results also shows that the maximum efficiency was obtained at an elapsed time of 8 h, and beyond this time the efficiency again decrease. The EN transients prove that regardless the inhibitor concentration, the steel was highly susceptible to localized corrosion.

Keywords Pipeline steel · EIS · EN · Sour corrosion · Inhibition efficiency

A. Torres-Islas (✉) · S. Serna · J. Uruchurtu · J. G. González-Rodríguez
UAEM, Centro de Investigacion en Ingeniería y Ciencias Aplicadas, Av. Universidad 1001, Col. Chamilpa, 62210 Cuernavaca, Morelos, Mexico
e-mail: atimarquis93@yahoo.com.mx

B. Campillo
UNAM, Facultad de Química/Instituto de Ciencias Físicas, Coyoacan, 04510 Mexico, DF, Mexico

1 Introduction

Corrosion is one of the most serious problems in the oil and gas industry, it produced environmental conditions such fluids with high concentrations of CO_2, H_2S and acids that in combination with water make these media highly corrosive. The conditions found are generally summarized as follows: anaerobic conditions, high concentration of carbon dioxide, salinity, and the presence of hydrogen sulfide (H_2S) [1–4]. In order to reduce the corrosion in steels in the oil and gas industry, the application of inhibitors is one of the most effective alternatives as an economical and flexible method for the protection of metallic surface against corrosion. Corrosion inhibitors are normally based on organic compounds, when added to a corrosive environment in very small concentrations, of the order of ppm, they can decrease significantly the corrosion rate of the exposed metal or alloy. The most common inhibition mechanism of organic inhibitors is their adsorption over metallic surfaces, it forms a protective barrier against corrosive agents contacting with metal [5]. Generally, the efficiency of an inhibitor to provide corrosion protection depends significantly upon the interactions between the inhibitor and the metal surface, and to certain extent it increases with the amount of the inhibitor added until a steady state is achieved beyond some inhibitor concentration limit [6, 7]. For instance, Singh [8] and Ateya et al. [9] showed that inhibition efficiency continuously increased with the inhibitor concentration up to a critical inhibitor concentration. Beyond this limit the inhibitor efficiency began to drop no matter the amount of inhibitor added. However, upon the corrosive media different inhibitors could have different performances.

The accelerating effect of H_2S on anodic dissolution of iron was investigated recently using alternating current

(AC) impedance and potentiostatic steady-state techniques [9, 10], X-ray diffraction and scanning electron microscopy [11]. A mechanism was proposed which includes a chemisorption step followed by two successive charge-transfer steps to interpret the anodic behavior of iron in acidic solutions containing H_2S [12]. On the other hand, there are several techniques that can be used for monitoring inhibition testing. However, few of them can be used to provide fundamental knowledge of corrosion and corrosion inhibition processes to develop better control methods for environmental corrosiveness. Electrochemical impedance spectroscopy (EIS) has been shown to be a powerful technique for studying inhibitor film formation and destruction processes, and for monitoring inhibitor film persistency [13, 14]. Also, electrochemical noise analysis ENA has been known as a convenient technique for continuously monitoring the corrosion process and inhibitor performance [15]. Although investigation in this field has been extensively, some discrepancies can be observed in the literature as reported by several other authors [16–21]. Meanwhile organic inhibitors based on Nitrogen, like imidazolines has been utilized successfully even though the protective mechanisms over metal surface is still uncertain and under debate [22]. Furthermore the corrosion imidazoline protective mechanisms can vary significantly related to the specifically material or alloy used. The aim of this work is to continue the study of corrosion inhibition performance of carboxyamidoimidazoline organic compounds by EIS and EN electrochemical techniques, in a new microalloyed high strength pipeline steel developed for sour service. In addition, the performance and inhibitor adsorption mechanism were analyzed by different adsorption isotherms models.

2 Experimental

2.1 Steel and test solution

The experimental microalloyed steel plates used in this study was classified as an API X80 grade microalloyed pipeline steel regarding their mechanical properties published elsewhere [23]. The steel chemical composition was analyzed by ISP technique with the following results in wt%: 0.044-C, 0.271-Si, 1.69-Mn, 0.0091-P, 0.0103-Cr, 0.240-Ni, 0.0010-V, 0.014-Ti, 0.2170-Cu, 0.25-Mo, 0.0310-Al, 0.0001-B, 0.0554-Nb–Fe balance. Steel plate testing specimens for the electrochemical tests were machined in the form of coupons with the following dimensions: 3 mm width, 5 mm length, and 2 mm thickness. Coupons were polished up to 600 grit silicon paper, rinsed with deionized water and degreased in acetone.

Electrochemical tests were carried out in a stirred testing solution, composed of NaCl (30 g/L) and acetic acid glacial (CH_3 COOH)-1.7 g/L with 3.52 g/L of sodium sulfide (Na_2S) added to simulate a saturated 500 mg/L of H_2S solution. The final measured pH solution was between 3.5 and 4, analytical grade reagents and deionized water were used obtaining a working volume of 100 mL. For each electrochemical test the testing solution was deareated by purging N_2 (99.95%) for 1 h, before adding CH_3COOH and the Na_2S reagent. The inhibitor compound used in this study was a carboxiamidoimidazoline, their general molecular structure was shown in Fig. 1. It consists of three different substructures: a nitrogen-containing a five-membered ring with two nitrogen elements, a pendant side chain with an active functional group, and a hydrocarbon chain. Also it is shown the chemical composition of the inhibitor used in each test, were n = 2, 3; x-OH/HN_2, R = n–$C_{17}H_{33}$ y RC (=0) $NH(CH_2)$ nX. The inhibitor concentrations tested were: 0, 5, 10, 25, 50 and 100 ppm. A sealed cell was used in both tests (ENA and EIS) with a vent to prevent over pressure during deaeration process. The cell was kept at 50 ± 2 °C by using a heating mantle. All the electrochemical experiments were performed at atmospheric pressure.

2.2 EIS measurements

A three-electrode test cell was used for EIS tests with a saturated calomel electrode (SCE) as reference electrode, a graphite rod as counter electrode and steel plate coupons as working electrodes. The electrochemical signals were monitored by AC Gill potentiostat connected to a personal computer. An alternating current (AC) signal, with an amplitude of 10 mV, was applied at the open-circuit potential (OCP) in the frequency range of 1 MHz to 10 kHz, in a period of 24 h acquiring data every 60 min. The microalloyed steel cupons were employed as working electrode, masked with acrylic enamel and embedded in polyacrylic resin. The samples were grinded up to 600 silicon grit paper, rinsed with deionized water and degreased with acetone. Immediately the specimens were immersed to the solution in the glass cell.

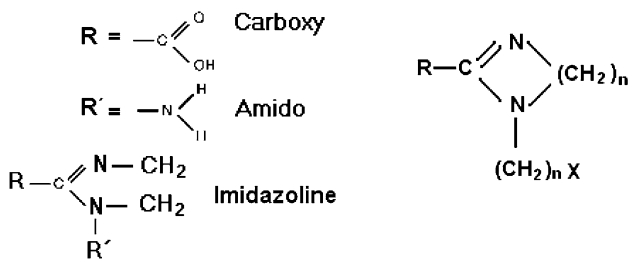

Fig. 1 Chemical structure of the carboxyamidoimidazoline used in this work

2.3 EN measurements

The experimental set-up used for electrochemical noise data recording, consisted of two identical working electrodes (steel plate coupons) and a SCE as reference electrode. The potential and current electrochemical noise fluctuations were recorded simultaneously. The data were obtained at one point per second in sequences of 2048 s during 24 h test period. The data was collected in an auto-ZRA ACM instrument connected to a personal computer. The noise resistance value (R_n) was obtained by statistical analysis of voltage and current noise records by Eq. 1 as follows:

$$R_n = \frac{\sigma[V(\Delta t)]}{\sigma[i(\Delta t)]} \quad (1)$$

where σ[V(Δt)] is the standard deviation of voltage noise at a time interval Δt and σ[i(Δt)] is the standard deviation of current noise in the same time interval Δt. Additionally, instantaneous noise resistance time series were obtained by dividing the voltage noise series by the current noise series. Removal of the DC trend from the raw noise data was the first step in the noise analysis. To accomplish this, a first order polynomial fitting was used. The DC trend has to be eliminated because this could originate large distortions in subsequent statistical noise data processing [15].

Equation 2 was used to obtain the fractional surface coverage (θ) due to the presence of the inhibitor molecules with respect to their concentration.

$$\theta = \frac{i_{corr}(blank) - i_{corr}(inhibited)}{i_{corr}(blank)} \quad (2)$$

where i_{corr} (*blank*) is the corrosion rate of the steel without inhibitor and i_{corr} (*inhibited*) is the corrosion rate in the presence of the inhibitor [16]. The corrosion rates were evaluated using noise resistance data and introducing their values in the Stern–Geary equation. Several adsorption models were considered as shown in Eqs. 3–6 for explaining the inhibitor adsorption mechanism
Temkin model:

$$K_{ad}C = e^{f\theta} \quad (3)$$

Langmuir model:

$$K_{ad}C = \frac{\theta}{1-\theta} \quad (4)$$

Freundlich model:

$$K_{ad}C^{1/n} = \theta \quad (5)$$

Frumkin model:

$$K_{ad}C = \left(\frac{\theta}{1-\theta}\right)e^{f\theta} \quad (6)$$

where K_{ad} is the adsorption equilibrium constant, C the concentration, θ is the fractional surface coverage as indicated in Eq. 2, and f is the molecular interaction constant.

3 Results and discussion

3.1 Electrochemical impedance spectroscopy

Nyquist and Bode (only phase angle-frequency) diagrams of the impedance spectra obtained for the immersed steel in test solution without inhibitor (blank condition), is shown in Fig 2. From the Nyquist plot (Fig. 2a) it can be observed that the impedance spectra exhibited a single capacitive like depressed semicircles. As the test time continues from 0 to 8 h the semicircle diameters was constantly growing. Decreased semicircles could be observed after 8 h, indicating an increment in the corrosion rate. Figure 2b shows a single phase angle shift at 1 MHz, then was shifted towards higher frequencies as time elapses. There is no

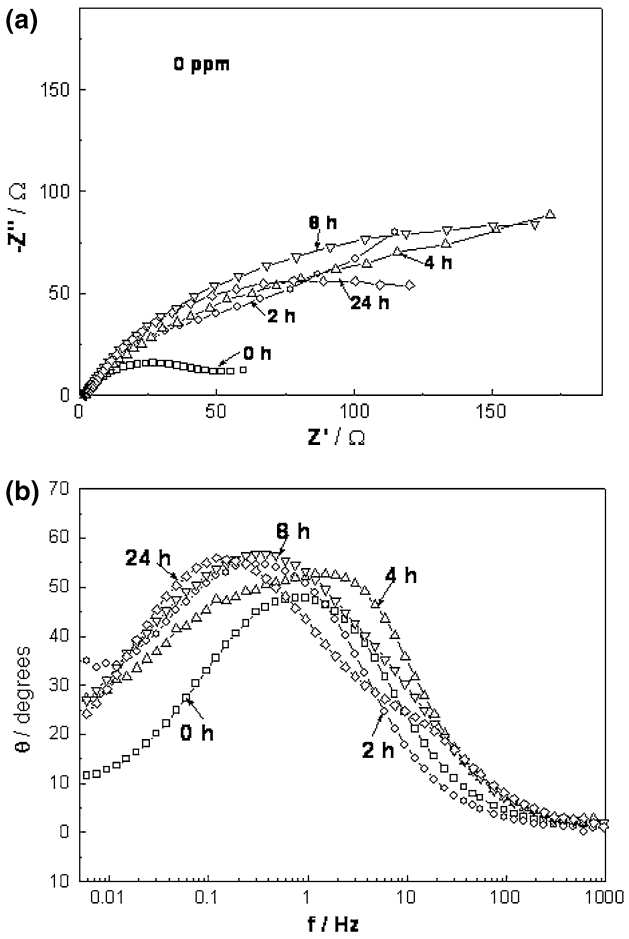

Fig. 2 Impedance spectra in the **a** Nyquist and **b** Bode representation for the blank condition at different testing times

evidence of the formation of a protective film because there is only one capacitive loop in the Nyquist plots [22]. The semicircles formed in the Nyquist diagram shows that the corrosion mechanism is under charge transfer control given by the two following electrochemical corrosion process.

The iron corrosion in presence of H_2S dissolved in water depends on the molecular H_2S dissociation, then iron becomes oxidized in the form of Fe^{++} (Eq. 7) and H_2S is being dissociated [24] as described in Eqs. 8–10. The final corrosion product combination became FeS as illustrated in Eq. 11.

Anodic reaction

$$Fe \rightarrow Fe^{++} + 2e^{-} \tag{7}$$

Cathodic reactions

$$H_2S + H_2O \rightarrow H^{+} + HS^{-}, \tag{8}$$

$$HS^{-} + H_2O \rightarrow H^{+} + S^{=} + H_2O, \tag{9}$$

$$2H^{+} + 2e^{-} \rightarrow H_2 \text{ or } 2H \tag{10}$$

Corrosion product combination

$$2e^{-} + 2H^{+} + Fe^{++} + S^{=} \rightarrow 2H + FeS \tag{11}$$

These reactions can be summarized by the following overall reaction:

$$Fe + H_2S \rightarrow FeS + 2H \text{ (in presence of } H_2O). \tag{12}$$

Due the low pH range used in the test solution in presence of H_2S and acetic acid, species like $FeSH^{+}$ exists. These species could form a ferrous sulfide corrosion product, known as Mackinawite [25], according to the following reaction:

$$FeSH^{+} \rightarrow Fe_{(1-x)} + xSH^{-} + (1-x)H^{+}. \tag{13}$$

Makinawite is a tetragonal sulfur-deficient iron sulfide with a composition of either FeS_{1-x} $(0 < x < 0.07)$ or $Fe_{1-x}S$ $(0.057 < x < 0.064)$ [26].

Other possible ferrous sulfide compounds can be formed (pirite and troilite) if a change in pressure, temperature or pH exists. The formation of these corrosion products has the tendency to form protective films. If inhibitor is added a film could be formed and anchored on top of these corrosion protective films, which in turn, will depend among other factors, like the microstructure of the steel. Depending of the FeS crystalline form this corrosion product could be precipitated into the test solution, or protect the steel surface. However, it could be possible the formation of Mackinawite in the blank condition steel surface the presence of a protective film was no evident as showed in Fig. 2 after 8 h of test. The continuous increment of the semicircle diameter up to 8 h could be explained in terms of a possible accumulation of the corrosion products with some protective characteristics. This

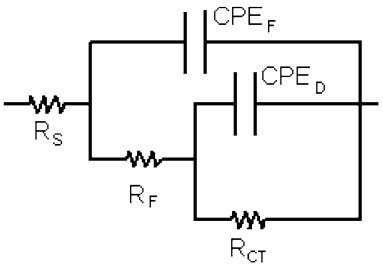

Fig. 3 Equivalent circuits used to model EIS data for uninhibited solution

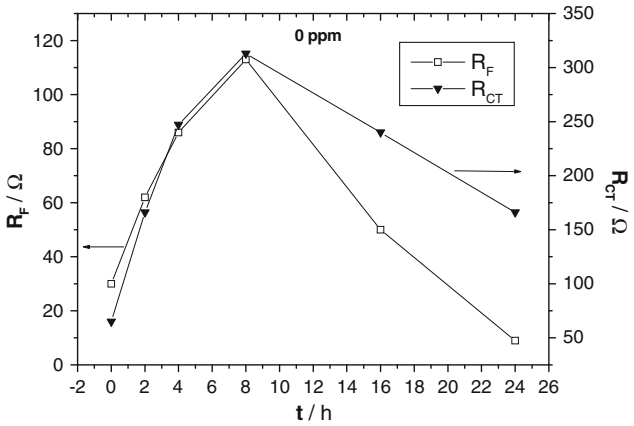

Fig. 4 Calculated values for R_F and R_{CT} for the blank solution

means that the protective effect in the H_2S solution can be related to the conjugated action of the FeS corrosion products and the inhibitor presence.

Figure 3 shows the equivalent electric circuit that simulates the impedance data showed in Fig. 2 where, R_s is the solution resistance, R_F is the resistance of the formed corrosion products film, CPE_F a constant phase element of the film, R_{CT} the charge transfer resistance, proportional to the semicircle diameter, and CPE_D is related to the capacitance of the double layer. R_F and R_{CT} calculated values from the equivalent circuit were shown on Fig. 4. In accordance with the data tendency showed in Fig. 2, their values have been incremented up to 8 h, after this time their values were decreased. The R_F and R_{CT} shows an important resistance values of 110 and near 300 Ω at 8 h, respectively, a suddenly fall of the resistance value was observed at 16 and 24 h, respectively, close to cero ohms (0 Ω) in the case of the R_F.

When 5 ppm of inhibitor was added as illustrated in Fig. 5a, the total impedance of the system increases during the first 8 h showing a continuous reduction as the immersion time continues until 24 h test. Similar to the 0 ppm (blank) condition, the impedance spectra showed depressed semicircles with centers located in the real axis,

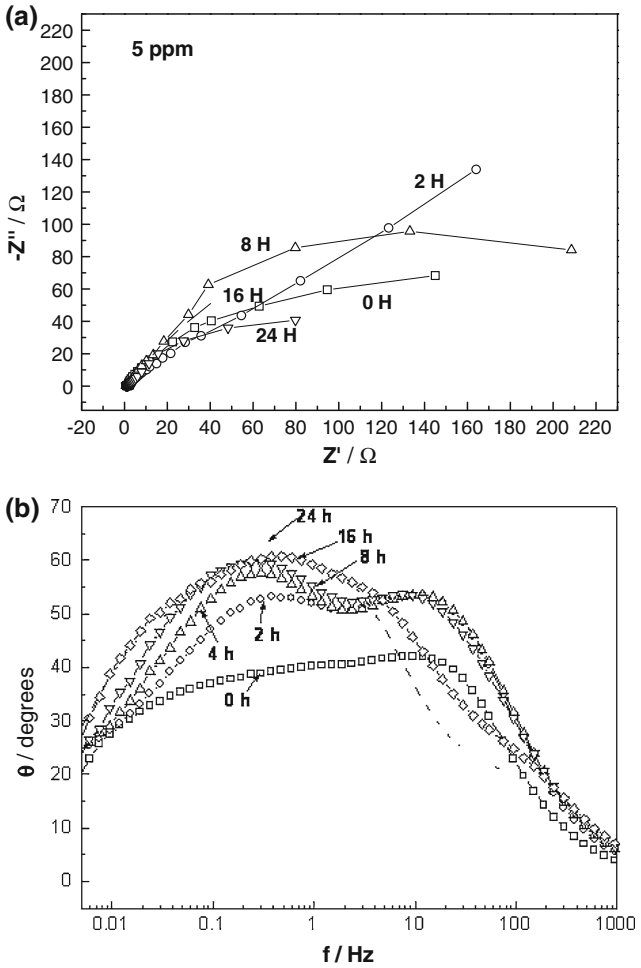

Fig. 5 Impedance spectra in the **a** Nyquist and **b** Bode representation for 5 ppm of inhibitor at different testing times

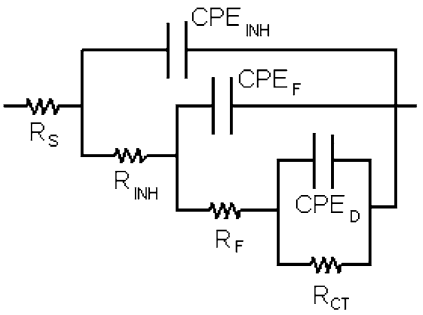

Fig. 6 Equivalent circuits used to model EIS data for inhibited solutions

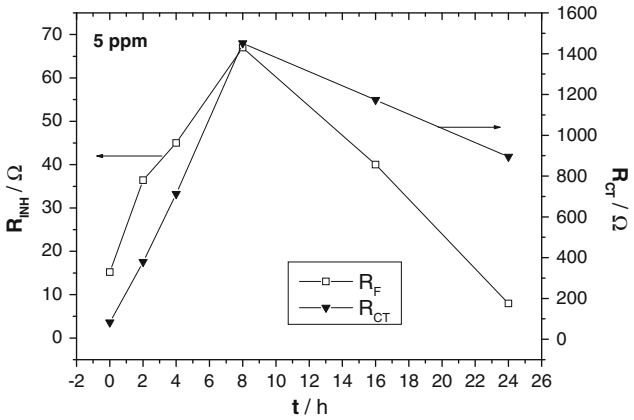

Fig. 7 Calculated values for R_{INH} and R_{CT} for the solution with 5 ppm of inhibitor

showing corrosion processes controlled mainly by a charge transfer process. The difference with the blank condition was observed in their Bode diagram (Fig. 5b) with two phase angle peaks at 20 and 0.3 Hz for lower times than 8 h. For longer times than 8 h there was only one peak at 0.3 Hz and was shifted towards lower frequencies as time elapses. The presence of these two peaks has been related with the formation of a protective film suggesting that this protective film is stable only for lower times (8 h) and afterwards the film could be degraded.

Figure 6 illustrates the equivalent electric circuit used to adjust the impedance experimental data for solutions with inhibitor additions. Where R_{INH} is the inhibitor formed film resistance and CPE_{INH} is related to its capacitance. Figure 7 shows R_{INH} and R_{CT} calculated values from the equivalent circuit showed in Fig. 6, it can be seen that their values has been raised with their respective increase in time until 8 h was reached. However, after this time both values decreased continuously. This means that the film is stable during the first 8 h, and the corrosion rate was also decreased. Beyond this time, the inhibitor losses its stability and the corrosion rate start to increase once again. Comparing the R_F and R_{INH} values tendency as shown in Figs. 4 and 7, it can be seen that both resistances shows the same behavior. Meaning that the inhibitor film could be anchored onto the corrosion products, but, in the case that the corrosion products were removed from the steel surface, the inhibitor film will be removed too.

The change in the impedance modulus with time for all the inhibitor concentrations is given in Fig. 8. Two general behaviors were observed: (i) the highest impedance modulus was reached with 5 ppm of inhibitor and then the impedance was decreased as the inhibitor concentration increases. The lower value was reached at the higher inhibitor concentration, similar to the impedance value found in the blank solution; (ii) the impedance modulus increases with elapsed time up to 8 h, after this time, the impedance modulus decreases continuously with elapsed time. The impedance spectroscopy results show that the lower corrosion rate was present when 5 ppm of inhibitor was added to the test solution then was incremented as the inhibitor concentration increases. Similarly, the corrosion rate decreases up to 8 h, and then it increases as time

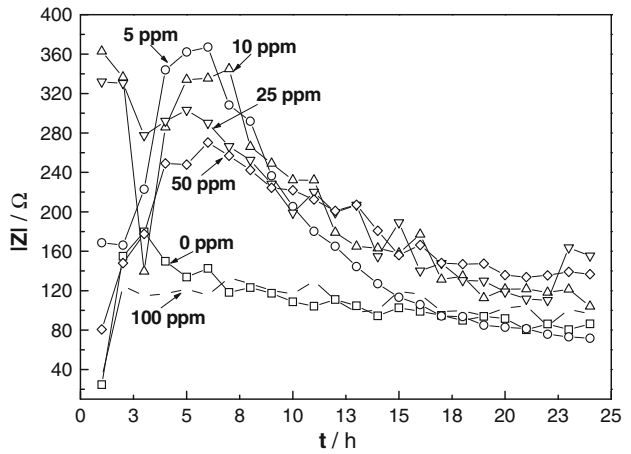

Fig. 8 Change in the impedance modulus with time for all the inhibitor concentrations used

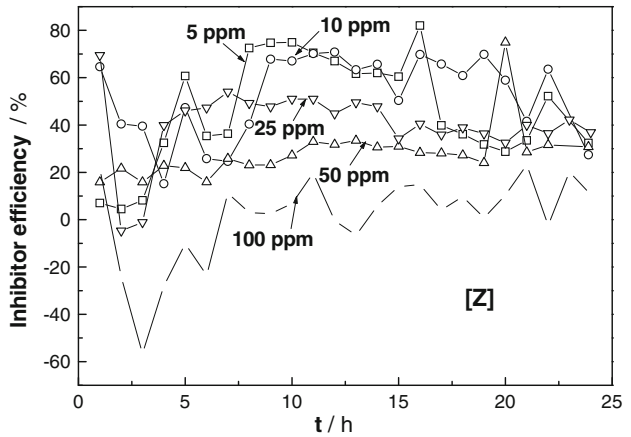

Fig. 9 Inhibitor efficiency as a function of inhibitor concentration using the [Z] values

continues. This behavior could be related to the inhibitive action as a function of the nature of the bond between the metal and the inhibitor [27]. Being this nature also a function of the functional group, related with the adsorption that increases with a decrease in electronegativity. The later is related to the increase in electron density of the functional group in the molecule which increases the hydrophobicity of the inhibitor.

Figure 9 shows the inhibitor concentration efficiency with respect to the test time, calculated using Eq. 2. This graph shows several stages and history behavior related to inhibitor concentration exposure time at the steel surface. At very early stages of corrosion, the most effective inhibitor concentrations were 10 and 25 ppm. Meanwhile at 5, 50 and 100 ppm the corrosion efficiency was very low and their respective corrosion efficiency values were very close. Indeed in accordance with previous results the worst behavior was showed at 100 ppm inhibitor concentration, including negative values which possibly mean that the corrosion rate is higher at 100 ppm than that obtained with the uninhibited solution. Showing, lower efficiency corrosion values than any other inhibitor concentration. It is remarkable the inhibitor efficiency behavior at 5 and 10 ppm concentrations (80%), but only in a well defined range of time between 8 and 18 h of test time. It is also clear that at 25 ppm inhibitor concentration and beyond the corrosion efficiency was worthless.

A question frequently asked regarding how often the batch treatment inhibitor should be repeated. EIS has been shown to be a useful technique for studying inhibitor film formation and destruction processes and for evaluating inhibitor film persistency. Inhibitor film persistency evaluation is essential for determining how often the batch treatment must be repeated and for optimizing the batch treatment procedures. The tendency of the studies over inhibitor film formation has been focused on the dependence of this film to the corrosion products layer previously formed, for instance, Rozenfield et al. [28], has been observed that inhibitors incorporate to corrosion product layer and forms a protective barrier between the base metal and the corrosive environment. French et al. [29] present results showing that the structure of the corrosion products is modified by the inhibitor presence. They have suggested that inhibitor structure has to be appropriated for their interaction with the corrosion products. Furthermore they report that imidazolines can be effective over iron sulfides and carbonates, but not over their oxides. The results presented by EIS technique (Figs. 2, 3, 4, 5, 6, 7, 8, 9) suggest that a batch treatment can be designed for microalloyed steels with this type of inhibitor concentrations between 5 and 10 ppm in sour environments at pH levels between 3.5 and 4 at 50 °C.

3.2 Electrochemical noise analysis

Figure 10 shows a continuous change in the noise resistance values (R_n) at all inhibitor concentrations. This figure shows a very similar behavior to that exhibited by the impedance modulus in Fig. 8, showing the higher R_n value and lowest corrosion rate at 5 ppm inhibitor concentration. Subsequently the R_n values decreases as the inhibitor concentration increases, showing the lower R_n values at 0 and 100 ppm inhibitor concentrations. The R_n maximum value for each inhibitor concentration, were achieved at a testing period of 8 h without considering the level of inhibitor concentration, consequently their respectively R_n value decreases continuously with time. The inhibitor efficiency calculated by using the R_n values showed a similar behavior to the inhibitor efficiency computed by using the impedance modulus as shown in Figs. 11 and 9, respectively.

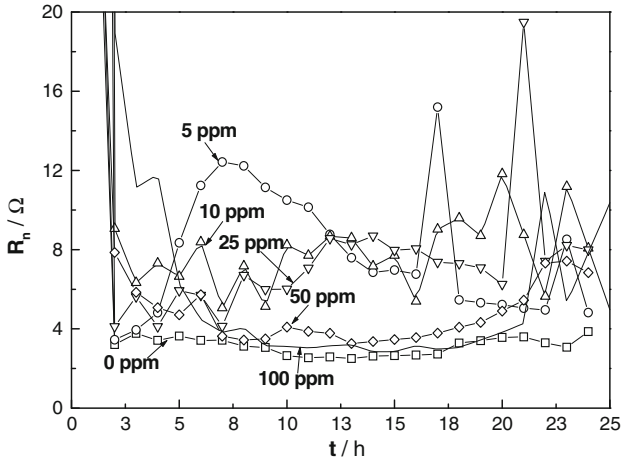

Fig. 10 Change in the noise resistance value, R_n; with time for all the inhibitor concentrations used

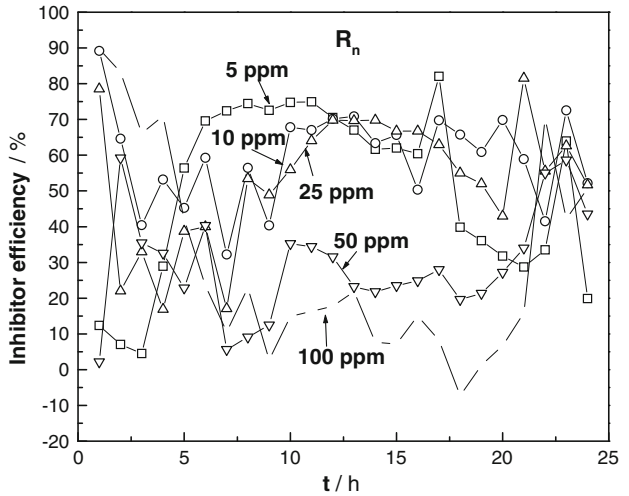

Fig. 11 Inhibitor efficiency as a function of inhibitor concentration using the R_n

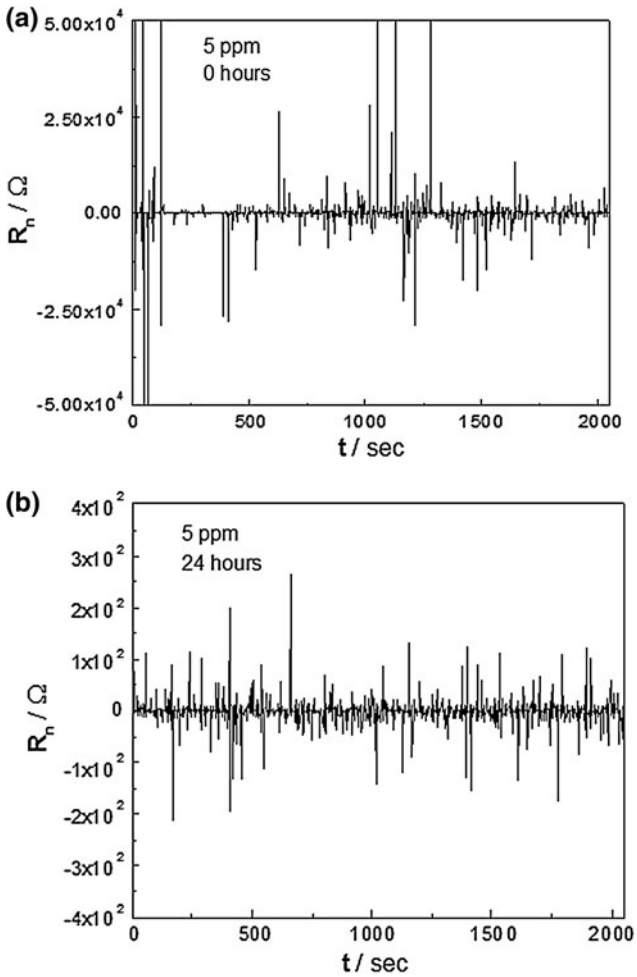

Fig. 12 Time series for the instantaneous R_n value for 0 ppm of inhibitor after **a** 0 and **b** 24 h of immersion

The result of dividing the instant noise voltage by the corresponding instant noise current is the instantaneous noise resistance, which is a better suited parameter for noise transient analysis. Figures 12 and 13 show the instantaneous noise resistance versus test time for 0 and 24 h of steel immersion time in the blank condition and 5 ppm inhibitor concentration respectively. The noise time series for the blank solution at the beginning of the test (Fig. 12a) shows negative and positive transients in the graph. Since two identical working electrodes were used, the negative transients can be related to the breaking of a formed film over the surface of one working electrode. The positive transients can be related to the burst of the film formed on the other identical working electrode. For the 24 h exposure time in the corrosive environment (Fig. 12b), these transients do not disappear and as shown, their intensities increased. This could be due to a permanent rupture of the corrosion product film over the steel surface.

When 5 ppm of inhibitor was added similar transients like those found in the uninhibited solution were observed in a similar frequency but with an intensity almost one order of magnitude lower, as shown in Fig. 13a. This could mean that the general corrosion rate was lowered but the localized type corrosion prevails. These transients are related to the inhibitor film formed over corrosion products. After 24 h of immersion (Fig. 13b), the transients was decreased two orders of magnitude, but also present a similar tendency towards localized corrosion. These transients were observed at all inhibitor concentrations, and were related to local rupture and restoring inhibitor film events.

Table 1 summarizes localized indexes (LI) for all the inhibitor concentrations at the beginning of the test and after 24 h of corrosive environment exposure. Regardless

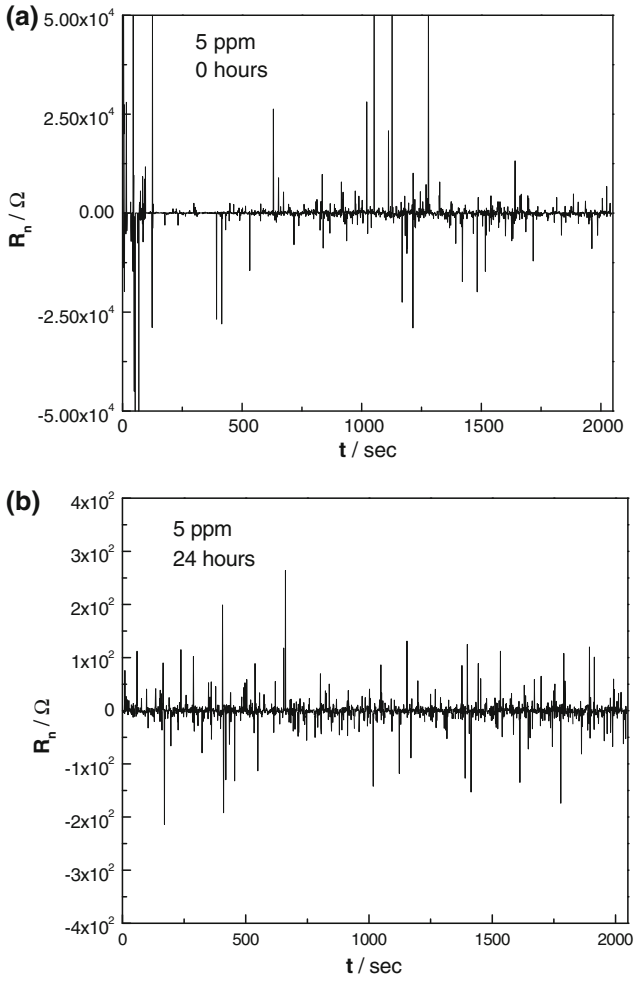

Fig. 13 Time series for the instantaneous R_n value for 5 ppm of inhibitor after **a** 0 and **b** 24 h of immersion

Table 1 Effect of inhibitor concentration on the localization index value after 0 and 24 h of testing

Inhibitor concentration (ppm)	Localization index	
	0 h	24 h
0	1.0002	0.999
5	1.0002	1.001
10	1.0002	0.999
25	0.999	1.003
50	1.0002	0.999
100	1.0004	1.0002

inhibitor concentration their LI values were close to unity which means that in all cases any film formed, by corrosion products, inhibitor coverage, or both could be broken. This result indicates that the steel was susceptible to localized corrosion at all environment conditions at 50 °C.

4 Summary and final discussion

The inhibitor film growth and persistency was detected by analyzing the EIS experimental data tendency and confirmed by the inhibitor efficiency estimation. The inhibitor film growth and persistency could be explained in terms of the imidazoline structure as follows. The head group and the $–CH_2–CH_2–NH_2$ pendant chain group of the imidazoline structure (Fig. 1), could promote a strong molecular bonding to the metal surface. This structure helps to improve their molecular adsorption [30] to the steel too in such a way that the film inhibitor was persistent during the whole monitoring period. This was evidenced by noise resistance (R_n) and the impedance modulus |Z| tendencies (Figs. 8, 10), respectively. However, Bode phase angle results indicated a low protection by the inhibitor that enables an electrochemical charge transfer process that takes place in the steel double-layer interface. This behavior was related to an inhibitor poor hydrophobic barrier and their hydrocarbon chain structure which in turn, can to a great extent affect inhibitor performance [7]. The inhibitor film generated allows the entry of water molecules that leads anodic and cathodic corrosion reactions promoting low protection to the steel surface. As discussed above, inhibitor film efficiency and deterioration is normally accompanied by typical changes in the Bode phase angle plots. Thus, the Bode phase angle diagram could be used as an indicator for monitoring inhibitor film behavior and can be used as a method for determining inhibitor film persistency.

Good agreement was obtained between the kinetic-thermodynamic and adsorption models. Correlation factor (R) values lower than unity was obtained employing Langmuir, Frumkin, Freundlich and Temkin models (Eqs. 4–6). However, Temkin isotherm shows an R value equal to 0.9515 as shown in Fig. 14, which was the highest

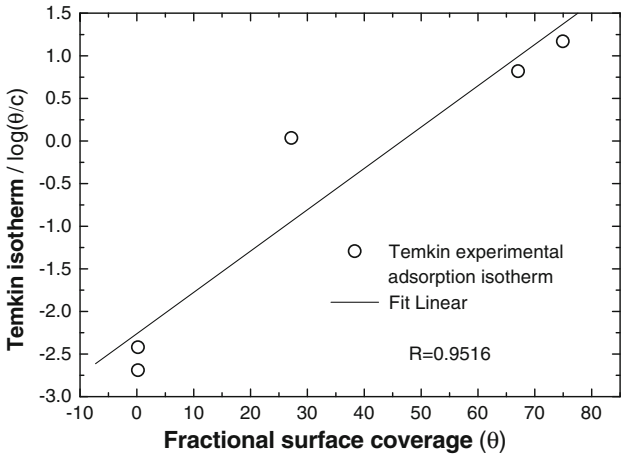

Fig. 14 Comparison between the experimental Temkin adsorption isotherm, and fit linear

correlation factor value obtained between all the considered isotherm models. The Fumkin isotherm model agreed only in cases where the active site occupancy or the relative-size parameters were equal to or close to unity. The Fumkin isotherm attempts to treat the deviations from the ideal Langmuir isotherm by the use of a lateral interaction parameter [31]. Temkin isotherm model (Eq. 3) attempt to explain the inhibitor film behavior related to the inhibitor adsorption mechanism on the steel surface suggesting that the more energetic sites are occupied first by the ions in solution. These occur once the ionic affinity falls linearly with their adsorption.

Unfortunately, the later results indicate that the inhibitor film barrier was not adequate for the steel protection under the H_2S corrosion environment condition tested. To prevent the system (steel-film inhibitor-environment) inhibitor protection decrease at all inhibitor concentrations, will be necessary to add more inhibitor (5–10 or 25 ppm) after 8 h indicating that his scenario does not represent the best result. However, the data obtained in the present work will give the possibility to reformulate the carboxyamidoimidazoline compound to make it more effective in the steel-environment system studied or for replacing it.

5 Conclusions

EIS and ENA were used successfully as combined techniques to study and evaluate the film behavior and persistency of carboxyamidomidazoline inhibitor film in an H_2S environment. Both techniques showed that for the micro alloyed steel assessed under sour environment conditions, the highest efficiency was obtained with 5 ppm of inhibitor and decreased as the inhibitor concentration increased. Furthermore, the film inhibitor efficiency initially increased as a function of time, than after some elapsed time their efficiency decreased. Noise resistance time series indicated that regardless the inhibitor concentration, the steel was highly susceptible towards localized type of corrosion due to film rupture events. Inhibitor adsorption mechanism can adequately be described by the Temkin isotherm.

Acknowledgements The authors acknowledge the financial support of Consejo Nacional de Ciencia y Tecnologia through "Programa de apoyo complementario para la consolidación institucional de grupos de investigacion" (Convocatoria 2006).

References

1. Tesseder RS (1981) Oil industry experience with hydrogen embrittlement and stress corrosion cracking. In: Tuttle RN, Kane RD (eds) H2S corrosion in oil and gas production—a compilation of classic papers. NACE, Houston, p 147
2. Kermani MB, Morshed A (2003) Corrosion 59:659
3. Videm K, Kvarekval J (1995) Corrosion 51:260
4. Hong T, Sun YH, Jepson WP (2002) Corros Sci 44:101
5. Sastri VS (1998) Corrosion inhibitors: principles and applications. Willey, New York
6. Ashassi-Sorkhabi H, Nabavi-Amri SA (2002) Electrochim Acta 47:2239
7. Chetouani A, Aouniti A, Hammouti B, Benchat N, Benhadda T, Kertit S (2003) Corros Sci 45:1675
8. Singh I (1993) Corrosion 49:473
9. Ateya BG, EI-Anadouli BE, EI-Nizamy FM (1984) Corros Sci 24:497
10. Huang H-H, Lee J-T, Tsai W-T (1999) Mat Chem Phys 58:177
11. Ren C, Liu D, Bai Z, Li T (2005) Mat Chem Phys 93:305
12. Veloz MA, Gonzalez I (2002) Electrochim Acta 48:135
13. Garcia LACJ, Jois CBJM, Cardoso EM, Mattos DR (2001) Electrochim Acta 46:3879
14. Cabrera-Sierra R, Sosa E, Pech-Canul MA, Gonzalez I (2006) Electrochim Acta 51:1534
15. Galicia P, Gonzalez I (2005) Electrochim Acta 50:4451
16. Durnie W, De Marco R, Jefferson A, Kinsella BJ (1999) Electrochem. Soc 146:1751
17. Ramachandran S, Jovancicevic V (1999) Corrosion 55:259
18. Arzola S, Mendoza-Florez J, Duran-Romero R, Genesca J (2006) Corrosion 62:433
19. Jovancicevic V, Ramachandran S, Prince P (1999) Corrosion 55:449
20. Cruz J, Martinez R, Genesca J, Garcia-Ochoa EJ (2004) Electroanal Chem 566:111
21. Rodriguez-Valdez LM, Martinez-Villafañe A, Golztman-Mitnik D (2004) Theochem 681:83
22. Xue-Yuan Z, Feng-Ping W, Yu-Fang H, Yuan-Long D (2001) Corros Sci 43:1417
23. Olivares I, Alanis M, Mendoza R, Campillo B, Juarez-Islas JA (2008) Ironmak Steelmak 6:453
24. Gerus BRD (1981) H_2S Corrosion in oil and gas production—a compilation of classic papers. NACE, Houston, p 888
25. Walter GW (1989) Corros Sci 26:681
26. Smith JS, Miller JDA (1975) Br Corros J 10:136
27. Gusmano G, Labella P, Montesperelli G, Privitera A, Tassinari S (2006) Corrosion 62:576
28. Rozenfel'd IL, Bogomolov DB, Gorodetskii AE, Kazanskii LP, Frolova LV, Shamova LI (1982) Protect Metals 18:121
29. French EC, Martin RL, Dougherty JA (1989) Mater Perform 28:46
30. Meyer FH, Riggs OL, McGlasson RL, Sudbury JD (1958) Corrosion 14:69
31. El-Awady AA, Abd-El-Nabey BA, Aziz SG (1992) J Electrochem Soc 139:2149